RSC Advances

PAPER

View Article Online
View Journal | View Issue

Cite this: *RSC Adv.*, 2019, **9**, 16863

Biological reduction of nitroimidazole-functionalized gold nanorods for photoacoustic imaging of tumor hypoxia†

Yui Umehara,[a] Toki Kageyama,[a] Aoi Son,[a] Yu Kimura,[a] Teruyuki Kondo *[a] and Kazuhito Tanabe *[b]

Received 5th February 2019
Accepted 15th May 2019

DOI: 10.1039/c9ra00951e

rsc.li/rsc-advances

Tumor-selective accumulation of gold nanorods (GNR) has been demonstrated for visualization of tumor hypoxia by photoacoustic imaging. We prepared GNRs with hypoxia-targeting nitroimidazole units (G-NI) on their surface. Biological experiments revealed that G-NI produced a strong photoacoustic signal in hypoxic tumor cells and tissues.

Hypoxia has attracted much attention as a typical feature of solid tumors.[1–5] Rapid proliferation of tumor cells and disproportionate angiogenesis cause an oxygen deficiency that produces hypoxic cells away from the blood vessels. Hypoxia has been closely associated with a malignant phenotype of cancer cells, resistance to cancer therapies, and low mortality rate of cancer patients,[6,7] and there is thus an increasing demand for methods to track these pathological cells.

Recently, several technologies including oxygen-responsive electrodes,[8,9] functional nanomaterials,[10–12] fluorescence[13–20] or phosphorescence emission[21–32] and magnetic resonance imaging (MRI)[33–36] have been adapted to visualize tumor hypoxia. Although these methods are useful for diagnosis, each has considerable limitations. For example, oxygen-responsive electrodes are invasive, and can measure the oxygen status in only a small region. Emission probes are highly sensitive to hypoxic cells, but the visualization of deep-seated pathological tissue is difficult because the emitted light does not permeate living tissues. MRI approaches require a large amount of probe to be administered to allow detection of oxygen levels. Thus, the development of a versatile detection system for tumor hypoxia remains a challenge.

In the past decade, photoacoustic imaging (PAI) has emerged as a promising modality for diagnosis.[37–39] Compared with optical imaging using fluorescence or phosphorescence, photoacoustic signals can penetrate more deeply into tissue, while maintaining high spatial resolution in biomedical imaging. In addition, PAI offers faster imaging than MRI. For application of PAI to diagnosis, plasmonic nanostructures, such as gold nanoparticles including nanorods (GNRs), nanoshells, and nanostars have been proposed as molecular probes, because they show robust photoacoustic signals.[40] These nanoparticles have been delivered to tumor tissue and modification of their surface allowed to visualize some receptors such as HER2, integrin, and EGFR by PAI.[41,42]

In light of these favorable features, we attempted to construct a molecular probe to detect tumor hypoxia by PAI using such gold nanoparticles. We employed GNRs as the PAI probe to target hypoxia because they can be excited by near-infrared light irradiation, which is preferred for bioimaging.[40] To visualize hypoxic tissue by PAI, we modified the GNRs with 2-nitroimidazole derivatives (NIs), which have the property of accumulating in hypoxic cells.[43–45] NIs are selectively reduced by nitroreductase under hypoxic conditions to form reactive products that bind irreversibly to cellular nucleophiles, resulting in their accumulation in hypoxic cells and regions. Therefore, we predicted that GNRs modified by NIs (G-NIs) would accumulate in hypoxic tumor tissue to show strong photoacoustic signals from this pathological tissue. Here, we report the preparation and characterization of G-NIs as PAI probe for tumor hypoxia.

The synthesis of G-NIs is summarized in Scheme 1. The GNRs were modified by polyethylene glycol that carried thiol and amino terminals (HS–PEG–NH_2), using the high affinity of the gold surface for thiol groups to give G-PEGs. Coupling of the amino groups of G-PEGs with the 2-nitroimidazole derivative, NI-CO_2H,[31,32] gave desired G-NIs. To confirm the immobilization of the NI units on the surface of the GNRs, FT-IR measurements were performed (Fig. 1A). The strong band at around 1100 cm^{-1} was assigned to the C–O–C stretching vibration of the aliphatic ether associated with PEG units.[46] It is

[a]Department of Energy and Hydrocarbon Chemistry, Graduate School of Engineering, Kyoto University, Nishikyo-ku, Kyoto, 615-8510, Japan. E-mail: teruyuki@scl.kyoto-u.ac.jp; Fax: +81-75-383-2504; Tel: +81-75-383-7055

[b]Department of Chemistry and Biological Science, College of Science and Engineering, Aoyama Gakuin University, 5-10-1 Fuchinobe, Chuo-ku, Sagamihara, 252-5258, Japan. E-mail: tanabe.kazuhito@chem.aoyama.ac.jp; Fax: +81-42-759-6493; Tel: +81-42-759-6229

† Electronic supplementary information (ESI) available. See DOI: 10.1039/c9ra00951e

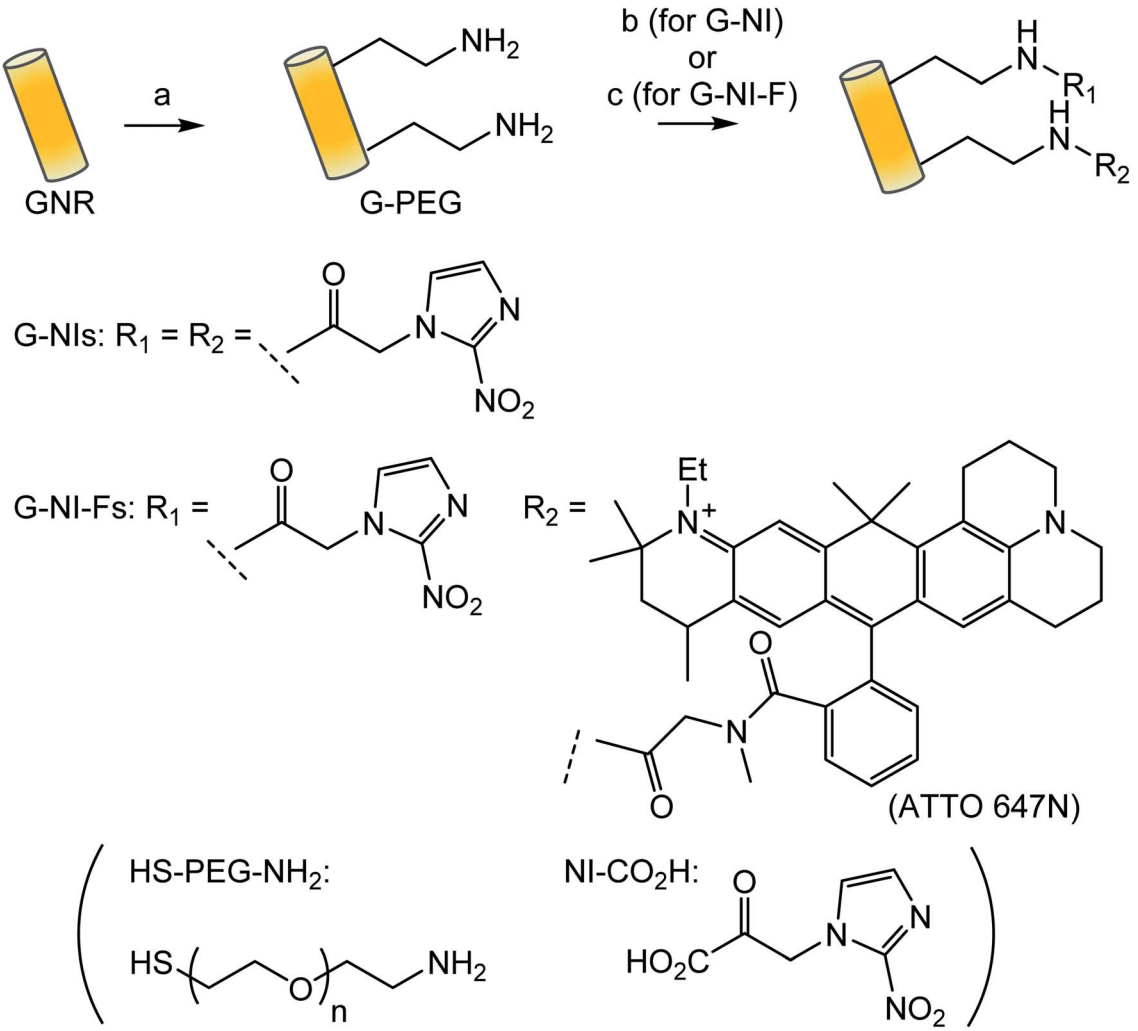

Scheme 1 Reagents and conditions: (a) HS–PEG–NH_2 (MW 5000), quant. (b) EDC, DMAP, HOBt, NI-CO_2H (c) EDC, DMAP, HOBt, NI-CO_2H, ATTO 647N NHS.

striking that the band around 1650 cm^{-1} observed for G-NIs was attributed to the C=O vibration[46] of the amide group, indicating that the NI units were immobilized on the surface of the GNRs. We also characterized the G-NIs by transmission electron microscopy (TEM) and absorption spectra. The TEM images of the nanoparticles indicated that the longitudinal and transverse lengths of G-NIs were 13 ± 1 nm and 36 ± 2 nm, respectively, and that their aspect ratio was 2.8. Absorption spectra revealed that modification of the surface of GNRs by PEG and NI units had a negligible effect on the size and shape of GNRs. Furthermore, measurement of the zeta potential value of nanoparticles verified that the GNR surface was modified. GNRs showed a negative charge (−13.5 ± 0.5 mV), while the charge of G-PEGs became positive (+4.9 ± 0.4 mV) because of the displacement of the surface molecules by PEG molecules bearing terminal amino groups. In addition, surface modification of G-PEGs by NI units to form G-NIs resulted in a decrease of their charge to +0.26 ± 0.2 mV, indicating that terminal amino groups were consumed to form an amide bond with NI-CO_2H. We also synthesized control nanoparticles bearing fluorescent ATTO-647 to give G-NI-Fs in a similar way (Scheme 1).

We next assessed the cytotoxic properties of G-NIs using the human lung carcinoma cell line A549. For the assessment of cytotoxicity, the cells were cultured for 24 h in the presence of various concentrations of G-NIs and then subjected to a cell viability assay (Fig. 2A). We confirmed that almost all of the cells had a high survival rate even in the presence of G-NIs up to 2.5 μM, indicating that G-NIs had low cytotoxicity in this concentration range. To evaluate the specific accumulation of G-NIs in hypoxic cells, we applied G-NI-Fs to the cellular imaging of A549 cells. The cells were pre-incubated under aerobic (20% O_2) or hypoxic (0.3% O_2) conditions for 24 h, followed by incubation with G-NI-Fs for 3 h. After washing, the cells were subjected to microscopy. As shown in Fig. 2B, there were significantly higher levels of G-NI-Fs fluorescence emission in the cells cultured under hypoxic conditions than in those cultured under aerobic conditions. Thus, G-NI-Fs was selectively retained in hypoxic cells.

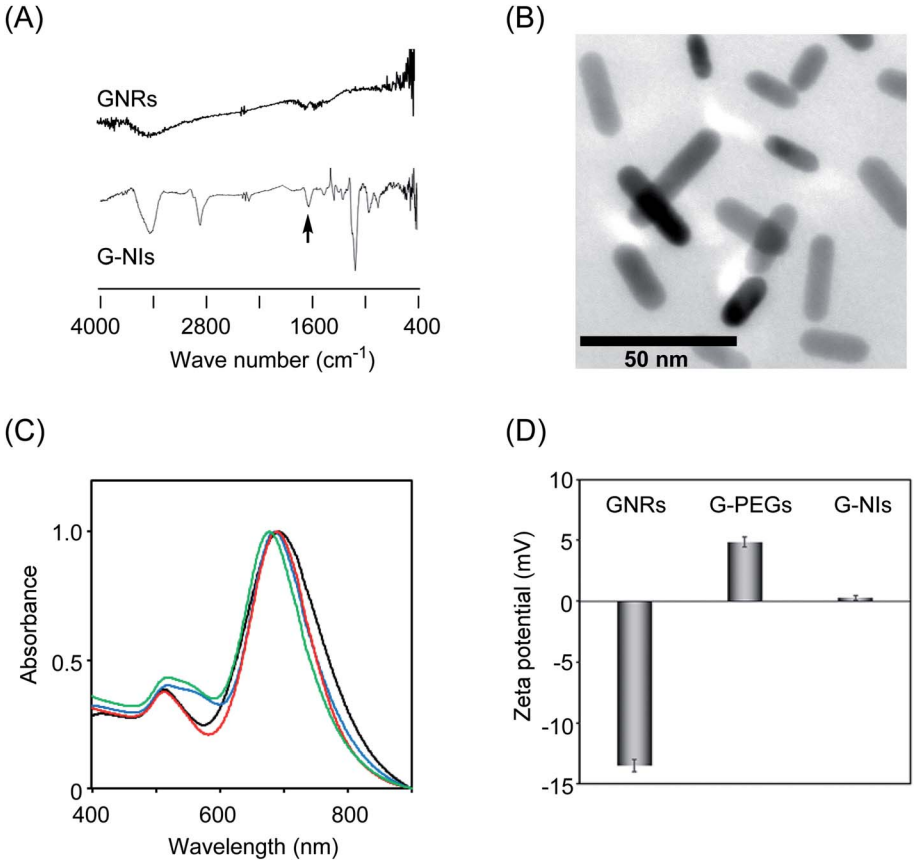

Fig. 1 (A) IR spectra of GNRs and G-NIs. Arrow indicates vibration of amide group. (B) Transition electron microscopic image of G-NIs. (C) Absorption spectra of GNRs (black line), G-PEGs (blue line), G-NIs (red line) and G-NI-Fs (green line) in aqueous solutions. (D) Zeta potential values of GNRs, G-PEGs and G-NIs.

Further assessment of accumulation of gold nanoparticles in A549 cells were conducted. The hypoxic cells were incubated in the presence of G-NI or G-PEG, and then the cell lysates were harvested for the measurement of ICP MS. The concentration of G-NI and G-PEG in hypoxic cells were estimated to be 1630 ± 427 and 111 ± 6 fmol per cell, respectively. The evidence that the amount of G-NI in aerobic cells was 120 ± 4 fmol per cell led to the conclusion that NI units on the nanoparticles are responsible for their accumulation in hypoxic cells. We next evaluated the effect of particle size on the cellular uptake. We newly synthesized small-sized gold nanorods with NI units (S-G-NI), the longitudinal and transverse lengths of which were 8 ± 3 nm and 20 ± 7 nm, respectively (Fig. S1†). As a control, we also synthesized small nanorods without NI units (S-G-PEG). The ICP MS measurements of cell lysate revealed that uptake of S-G-NI in hypoxic cells was highly efficient (*ca.* 16 pmol per cell), but S-G-PEG also accumulated in hypoxic cells with moderate efficiency (*ca.* 7.7 pmol per cell). Thus, the small G-NI had low selectivity toward hypoxic cells. In addition, recent report showed that gold nanoparticles with large size (*ca.* 120 nm) had low cellular uptake.[47] In light of these properties, we presumed that the gold nanoparticles with size of *ca.* 40 nm is favorable for molecular imaging of hypoxic cells.

The intracellular localization of the nanoparticles was evaluated using G-NI-Fs and several tracking reagents to conduct multicolor imaging. We merged the images of G-NI-Fs fluorescence with that of cytoplasmic organelle-specific fluorescence molecules targeting lysosomes, mitochondria, and endoplasmic reticulum (ER) (Fig. S2†). We observed a merged yellow color for G-NI-Fs and fluorescent agents targeting lysosomes and ER, while the mitochondria-targeting fluorescent agent did not give any merged signal. Thus, nanoparticles seem to have efficient access to the lysosome and ER in the cytoplasm. We also evaluated TEM images of A549 cells that were incubated with G-NIs, and confirmed that G-NIs accumulated in the cell vacuoles (Fig. 2D).

Further attempts were made to visualize hypoxic tumor cells in mice using PAI. For the imaging of tumor tissue, we selected colon 26 cells and transplanted them into the lower thigh of nude mice, because these cells are widely used for the study of tumor hypoxia *in vivo*. After the tumor grew to 5 mm in size, G-NIs in saline (5 pmol) were administered intravenously. As shown in Fig. 3A, obvious photoacoustic signals were obtained from the tumor tissue 24 h after injection of G-NIs. Given that injection of the control G-PEGs, which did not have NI units, led to only ambiguous images, G-NIs accumulated in hypoxic tumor cells in mice due to the function of their NI units. In

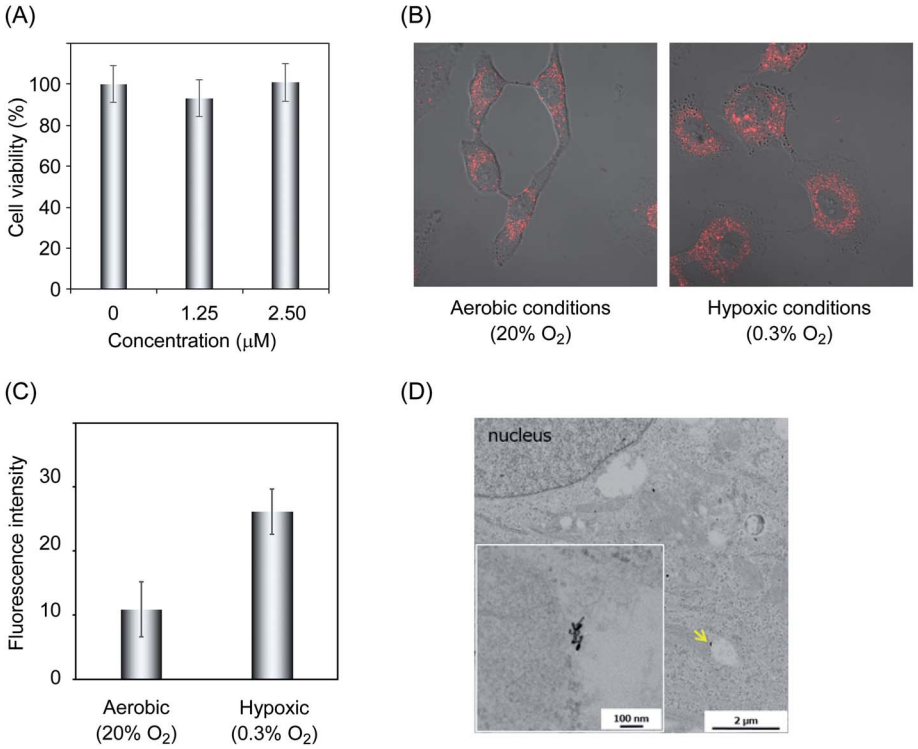

Fig. 2 (A) Cell viability assay of A549 cells in the presence of G-NI for 24 h. (B) Confocal microscopic images of A549 cells treated by G-NI-Fs. The cells were incubated in aerobic (20% O_2) or hypoxic (0.3% O_2) conditions. (C) The fluorescence intensity obtained from each cells in (B) were shown. (D) Transition electron microscopy image of A549 cell incubated with G-NIs for 24 h. Arrows indicate the nanoparticles in the cell vacuoles. Magnified picture was also shown.

a separate experiment, we performed ex vivo imaging using G-NI-Fs, and confirmed robust emission from G-NI-Fs in tumor tissue as well as in liver and kidney (Fig. S3†). We next evaluated the effect of PEG units in G-NIs on the accelerated blood clearance (ABC) phenomenon.[48] The amount of anti-PEG IgM was measured by ELISA after the injection of G-NIs, G-PEGs or GNRs to mice. Although slight amount of anti-PEG IgM in serum was produced after administration of G-NIs (Fig. 4), this level was much lower than that produced after G-PEGs administration. A clear image of tumor tissue was obtained even after

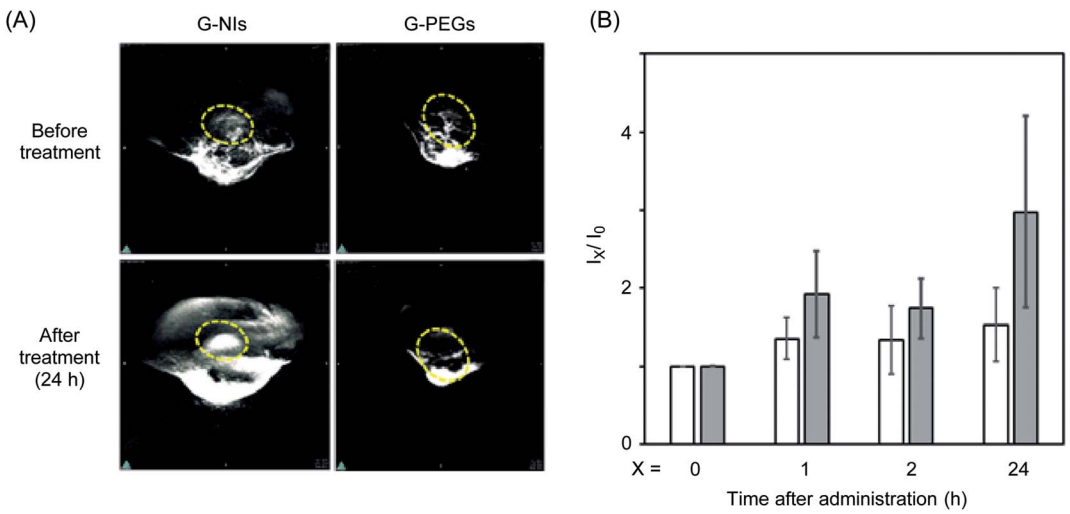

Fig. 3 (A) Photoacoustic images of tumor (colon 26) bearing mice. The images were obtained before injection or at 24 h after injection of G-NIs or G-PEGs. Yellow circles indicate the position of tumor tissue. (B) Ratio of photoacoustic signal intensity ($I_{24\ h}/I_{0\ h}$: $I_{24\ h}$ indicate photoacoustic signal intensity at 24 h after administration of G-NIs or G-PEGs, and $I_{0\ h}$ indicates signal intensity before administration) after injection of G-NIs (gray) or G-PEGs (white). The signal intensities were measured at designated time after injection (0, 1, 2 and 24 h).

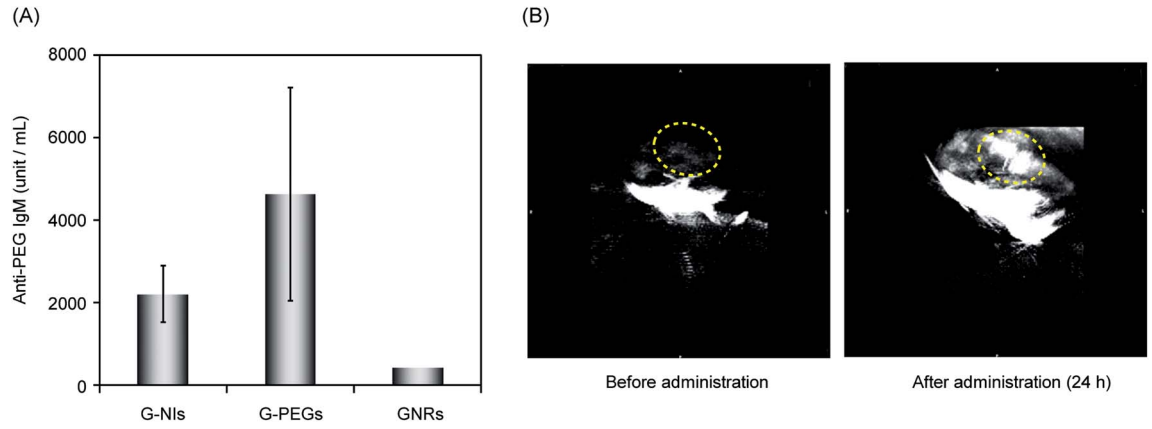

Fig. 4 (A) Generation of anti-PEG IgM after administration of G-NIs, G-PEGs or GNRs to mice. After their blood were collected, the anti-PEG IgM was determined by ELIZA. (B) Photoacoustic images of tumor (colon 26) bearing mice after second injection of G-NIs. The images were obtained before injection or at 24 h after injection of G-NIs. Yellow circles indicate the position of tumor tissue.

the second injection of G-NIs (Fig. 4B), indicating that the effect of clearance of nanoparticles on PAI was negligible. Thus, it is reasonable to conclude that G-NIs possessed appropriate properties for visualization of hypoxic tumor tissue by PAI.

Ethical statement

All studies and procedures were approved by Animal Research Committee of Kyoto University Graduate School of Medicine. All animal experiments were performed according to the Institutional Guidance of Kyoto University on Animal Experimentation and under permission by the animal experiment committee of Kyoto University.

Conclusion

In summary, we synthesized GNRs bearing NI units on their surface (G-NIs) and characterized their properties as an indicator of hypoxia for PAI. GNRs showed a strong photoacoustic signal, and the tethering of NI units to nanoparticles resulted in their accumulation in hypoxic cells and tissues because of the reduction properties of NIs by intracellular reductases. Thus, G-NI was permitted to accumulate in the hypoxic cells to show their photoacoustic signals in hypoxic tumor cells and tissues. This nano-sized probe, G-NIs, is a promising photoacoustic probe for tracking tumor hypoxia.

Conflicts of interest

There are no conflicts to declare.

Acknowledgements

This work was supported in part by Grant-in-Aid for Scientific Research (for K. T. Grant number 23113508, and for T. K. Grant numbers 15K01819 and 17H05528), Grant-in-Aid for Challenging Exploratory Research (for A. S. Grant number 16K12876), Grant-in-Aid for JSPS Fellows (for Y. U. Grant number 17J03866) and the Innovative Techno-Hub for Integrated Medical Bio-Imaging of the Project for Developing Innovation Systems from the Ministry of Education, Culture, Sports, Science and Technology (MEXT), Japan. T. K. and A. S. acknowledge financial support from the Acceleration Transformative Research for Medical Innovation (ACT-M) from the Japan Agency for Medical Research and Development (AMED).

References

1 A. G. Anastasidadis, B. C. Stisser, M. A. Ghafer, M. Buchardt and R. Buttyan, *Curr Urol Rep.*, 2002, **3**, 222–228.
2 J. M. Brown and W. R. Wilson, *Nat. Rev. Cancer*, 2004, **4**, 437–447.
3 X. Zhang, Z. Xi, J. O. Machuki, J. Luo, D. Yang, J. Li, W. Cai, Y. Yang, L. Zhang, J. Tian, K. Guo, Y. Yu and F. Gao, *ACS Nano*, 2019, DOI: 10.1021/acsnano.8b09786.
4 W. Zhang, S. Li, X. Liu, C. Yang, N. Hu, L. Dou, B. Zhao, Q. Zhang, Y. Suo and J. Wang, *Adv. Funct. Mater.*, 2018, **28**, 1706375.
5 F. Koga, K. Takemura and H. Fukushima, *Int. J. Mol. Sci.*, 2018, **19**, 2777.
6 A. L. Harris, *Nat. Rev. Cancer*, 2002, **2**, 38–47.
7 S. Kizaka-Kondoh, M. Inoue, H. Harada and M. Hiraoka, *Cancer Sci.*, 2003, **94**, 1021–1028.
8 R. D. Braun, J. L. Lanzen and M. W. Dewhirst, *Am. J. Physiol.*, 1999, **277**, H551.
9 J. Lanzen, R. D. Braun, B. Klitzman, D. Brizel, T. W. Secomb and M. W. Dewhirst, *Cancer Res.*, 2006, **66**, 2219–2223.
10 J. Liu, Z. Liu and D. Wu, *Int. J. Med.*, 2019, **14**, 707–719.
11 J. Pang, R. G. Mendes, A. Bachmatiuk, L. Zhao, H. Q. Ta, T. Gemming, H. Liu, A. Liu and M. H. Rummeli, *Chem. Soc. Rev.*, 2019, **48**, 72–133.
12 K. Olszowska, J. Pang, P. S. Wrobel, L. Zhao, H. Q. Ta, Z. Liu, B. Trzebicka, A. Bachmatiuk and M. H. Rummeli, *Synth. Met.*, 2017, **234**, 53–85.

13 Y. Liu, Y. F. Xu, X. H. Qian, Y. Xiao, J. W. Liu, L. Y. Shen, J. H. Li and Y. X. Zhang, *Bioorg. Med. Chem. Lett.*, 2006, **16**, 1562–1566.
14 Y. Liu, Y. F. Xu, X. H. Qian, J. W. Liu, L. Y. Shen, J. H. Li and Y. X. Zhang, *Bioorg. Med. Chem.*, 2006, **14**, 2935–2941.
15 R. J. Hodgkiss, R. W. Middleton, J. Parrick, H. K. Rami, P. Wardman and G. D. Wilson, *J. Med. Chem.*, 1992, **35**, 1920–1926.
16 K. Tanabe, N. Hirata, H. Harada, M. Hiraoka and S. Nishimoto, *ChemBioChem*, 2008, **9**, 426–432.
17 E. Nakata, Y. Yukimachi, H. Kariyazono, S. Im, C. Abe, Y. Uto, H. Maezawa, T. Hashimoto, Y. Okamoto and H. Hori, *Bioorg. Med. Chem.*, 2009, **17**, 6952–6958.
18 K. Kiyose, K. Hanaoka, D. Oushiki, T. Nakamura, M. Kajimura, M. Suematsu, H. Nishimatsu, T. Yamane, T. Terai, Y. Hirata and T. Nagano, *J. Am. Chem. Soc.*, 2010, **132**, 15846–15848.
19 H. Komatsu, K. Tanabe and S. Nishimoto, *Bioorg. Med. Chem. Lett.*, 2011, **21**, 790–793.
20 K. Okuda, Y. Okabe, T. Kadonosono, T. Ueno, B. G. M. Youssif, S. Kizaka-Kondo and H. Nagasawa, *Bioconjugate Chem.*, 2012, **23**, 324–329.
21 K. K.-W. Lo and S. P.-Y. Li, *RSC Adv.*, 2014, **4**, 10560–10585.
22 A. Fercher, S. M. Borisov, A. V. Zhdanov, I. Klimant and D. B. Papkovsky, *ACS Nano*, 2011, **5**, 5499–5508.
23 R. I. Dmitriev, A. V. Zhdanov, G. Jasionek and D. B. Papkovsky, *Anal. Chem.*, 2012, **84**, 2930–2938.
24 S. Zhang, M. Hosaka, T. Yoshihara, K. Negishi, Y. Iida, S. Tobita and T. Takeuchi, *Cancer Res.*, 2010, **70**, 4490–4498.
25 O. Mazuryk, M. Maciuszek, G. Stochel, F. Suzenet and M. Brindell, *J. Inorg. Biochem.*, 2014, **134**, 83–91.
26 N. W. Choi, S. S. Verbridge, R. M. Williams, J. Chen, J.-Y. Kim, R. Schmehl, C. E. Farnum, W. R. Zipfel, C. Fischbach and A. D. Stroock, *Biomaterials*, 2012, **33**, 2710–2722.
27 R. Lincoln, L. Kohler, S. Monro, H. Yin, M. Stephenson, R. Zong, A. Chouai, C. Dorsey, R. Hennigar, R. P. Thummel and S. A. McFarland, *J. Am. Chem. Soc.*, 2013, **135**, 17161–17175.
28 H. Kurokawa, H. Ito, M. Inoue, K. Tabata, Y. Sato, K. Yamagata, S. Kizaka-Kondoh, T. Kadonosono, S. Yano, M. Inoue and T. Kamachi, *Sci. Rep.*, 2015, **5**, 10657.
29 H. Komatsu, K. Yoshihara, H. Yamada, Y. Kimura, A. Son, S. Nishimoto and K. Tanabe, *Chem.–Eur. J.*, 2013, **19**, 1971–1977.
30 R. Kurihara, R. Ikegami, W. Asahi and K. Tanabe, *Bioorg. Med. Chem.*, 2018, **26**, 4595–4601.
31 A. Son, A. Kawasaki, D. Hara, T. Ito and K. Tanabe, *Chem.–Eur. J.*, 2015, **21**, 2527–2536.
32 K. Yoshihara, K. Takagi, A. Son, R. Kurihara and K. Tanabe, *ChemBioChem*, 2017, **18**, 1650–1658.
33 C. Baudelet, G. O. Cron, R. Ansiaux, N. Crokart, J. DeWever, O. Feron and B. Gallez, *NMR Biomed.*, 2006, **19**, 69–76.
34 C. Baudelet, R. Ansiaux, B. F. Jordan, X. Havaux, B. Macq and B. Gallez, *Phys. Med. Biol.*, 2004, **49**, 3389–3412.
35 K. Tanabe, H. Harada, M. Narazaki, K. Tanaka, K. Inafuku, H. Komatsu, T. Ito, H. Yamada, Y. Chujo, T. Matsuda, M. Hiraoka and S. Nishimoto, *J. Am. Chem. Soc.*, 2009, **131**, 15982–15983.
36 S. Iwaki, K. Hanaoka, W. Piao, T. Ueno and T. Nagano, *Bioorg. Med. Chem. Lett.*, 2012, **22**, 2798–2802.
37 J. Weber, P. C. Beard and S. E. Bohndiek, *Nat. Methods*, 2016, **13**, 639–650.
38 C. Kim, C. Favazza and L. V. Wang, *Chem. Rev.*, 2010, **110**, 2756–2782.
39 B. R. Smith and S. S. Gambhir, *Chem. Rev.*, 2017, **117**, 901–986.
40 W. Li and X. Chen, *Nanomedicine*, 2015, **10**, 299–320.
41 L. Nie, S. Wang, X. Wang, P. Rong, Y. Ma, G. Liu, P. Huang, G. Lu and X. Chen, *Small*, 2014, **10**, 1585–1593.
42 H. Shi, Z. Wang, C. Huang, X. Gu, T. Jia, A. Zhang, Z. Wu, L. Zhu, X. Luo, X. Zhao, N. Jia and F. Miao, *Small*, 2016, **12**, 3995–4006.
43 N. K. Wagh, Z. Zhou, S. M. Ogbomo, W. Shi, S. K. Brusnahan and J. C. Garrison, *Bioconjugate Chem.*, 2012, **23**, 527–537.
44 S. K. Chitneni, G. M. Palmer, M. R. Salutsky and M. W. Dewhirst, *J. Nucl. Med.*, 2012, **52**, 165–168.
45 M. Mallia, C. Kumar, A. Mathur, H. D. Sarma and S. Banerjee, *Nucl. Med. Biol.*, 2012, **39**, 1236–1242.
46 R. M. Silverstein and F. X. Webster, *Spectrometric Identification of Organic Compounds*, John Wiley & Sons, Inc., 1998.
47 Y.-S. Chen, Y. Zhao, S. J. Yoon, S. S. Gambhir and S. Emelianov, *Nat. Nanotechnol.*, 2019, **14**, 465–472.
48 X. Wang, T. Ishida and H. Kiwada, *J. Control. Release*, 2007, **119**, 236–244.